J Solid State Electrochem (2008) 12:961–969
DOI 10.1007/s10008-007-0438-6

ORIGINAL PAPER

Olivine-type nanoparticle for hybrid supercapacitors

Rajaraman Vasanthi · Dharmalingan Kalpana · Nedumaram Gopalan Renganathan

Received: 19 July 2007 / Revised: 10 September 2007 / Accepted: 27 September 2007 / Published online: 7 November 2007

Abstract $LiCoPO_4$ nanoparticles were precipitated from polyethylene glycol solution of lithium acetate, cobalt acetate, and ammonium dihydrogen phosphate by refluxing at 250 °C for 35 h. The resultant powder samples were heated at 800 °C for different time periods of 2 and 4 h to study the effect of annealing time on the growth of samples. The X-ray diffraction pattern of the obtained samples exhibited olivine phase. The scanning electron microscopic images of dried powder sample and samples heated at 800 °C for 2 and 4 h showed a homogenous orthorhombic morphology with a particle size of few nanometers range. For the first time, orthorhombic olivine was introduced as positive electrode for a hybrid electrochemical supercapacitor cell with carbon nanofoam as negative electrode in 1 M $LiClO_4$ in ethylene carbonate and propylene carbonate (1:1 in volume) solution. A sloping voltage profile of 2 to 0 V is observed for all the three hybrid cells. From the impedance results, we inferred that $LiCoPO_4$ nanoparticles synthesized by polyol process offers less resistance than lithium titanium oxide. According to the results of electrochemical testing for the first time, maximum power density of 192 W/kg at 11 Wh/kg energy density was obtained for $LiCoPO_4$ nanoparticles annealed at 800 °C for 2 h. The dried sample and the sample heated at 800 °C for 2 and 4 h exhibited high capacitances of 5, 19, and 4 F/g, respectively, with an excellent rate capability over 1,000 cycles.

Keywords $LiCoPO_4$ · Olivine · Hybrid supercapacitor · Carbon nanofoam · Energy Density · Power density

Contribution to ICMAT 2007, Symposium K: Nanostructured and bulk materials for electrochemical power sources, July 1–6, 2007, Singapore.

R. Vasanthi (✉) · D. Kalpana
Electrodics and Electrocatalysis,
Central ElectroChemical Research Institute,
Karaikudi 630 006 Tamilnadu, India
e-mail: vasanthi_rajaram@yahoo.com

N. G. Renganathan
Lithium Batteries Division,
Central ElectroChemical Research Institute,
Karaikudi 630 006 Tamilnadu, India

Introduction

The characteristics of high capacity values in farads range and low in resistance are devices required for application in high current loads. To meet this requirement, higher energy density (150–200 Wh/kg) realized by Li ion batteries [1] and higher power density (5,000 W/kg) by carbon–carbon double-layer capacitor [2] shall be combined together to yield hybrid supercapacitor. This essentially consists of an electrochemical double-layer capacitor (EDLC) electrode and a battery electrode, such as (AC)/$Ni(OH)_2$ aqueous cell [3] or AC/$Li_4Ti_5O_{12}$ non-aqueous cell [4]. Amatucci et. al. [5] and Pasquier et. al. [6] have explored non-aqueous hybrid devices with Li intercalation anode, $Li_4Ti_5O_{12}$, and Wang et. al. [7, 8] worked on $LiMn_2O_4$, $LiCoO_2$, and $LiCo_{1/3}Ni_{1/3}Mn_{1/3}O_2$ in aqueous system. To our knowledge, this is the first attempt to use lithium metal phosphates with ordered-olivine structure for hybrid supercapacitor. To date, $LiCoPO_4$ has been prepared in different routes like sol-gel synthesis, solid-state reaction, hydrothermal synthesis [9–11], etc., to yield a pure phase. A new method to obtain nanoparticles with pure phase had been achieved by polyol process [12]. Polyol process has been widely used to synthesize metal colloid in which polyol is

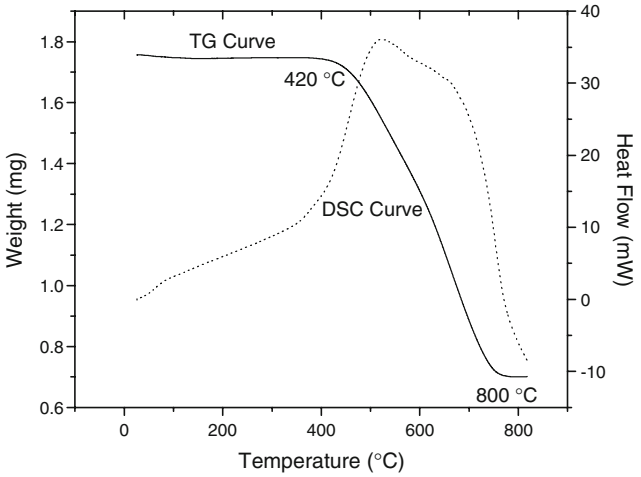

Fig. 1 TG-DSC curve for $LiCoPO_4$ nanoparticles

used as solvent reducing agent. Polyethylene glycol (PEG) is used in this method. General mechanism is that the ethylene glycol decomposes to generate reducing species for the reduction of the metal ions to metallic particles at high temperature. $LiCoPO_4$ particles are formed at 250 °C, boiling point of PEG.

In the present paper, we describe the synthesis of nano crystalline $LiCoPO_4$ using polyol process followed by annealing the dried sample at 800 °C for different time periods of 2 and 4 h to study the effect of annealing time on the growth of samples. The electrochemical property of the prepared dried sample, samples annealed at 800 °C for 2 and 4 h in supercapacitors, are presented. $LiCoPO_4$ pristine (without carbon coating) was introduced as positive electrode for a hybrid electrochemical supercapacitor with carbon nanofoam, CNF (surface area 1,500 m^2/g, specific capacitance 30 F/g), as negative electrode in 1 M $LiClO_4$ in ethylene carbonate (EC) and propylene carbonate (PC) (1:1 in volume) solution. This is to assess the capacitance of the pristine electrode in $LiClO_4$ in EC/PC, non-aqueous electrolyte, which is used with a view to increase the working voltage and also increase of energy density of the battery electrode material. This will result in a significant increase in the overall energy density of the capacitors compared with that of EDLCs. In these systems, one electrode stores a charge through reversible non-faradic reactions in a transition metal oxide or lithium ion intercalated compound. The charge /discharge process is associated with the transfer of Li ions between two electrodes. The electrolyte mainly plays the role of ionic conductor. In the reactions of the hybrid supercapacitor formed with CNF/$LiCoPO_4$, cations and anions separate during the charge process. Charge stored at both electrodes should be balanced and equal the charge of ions consumed from the electrolyte. The electrolyte depletion problem limits greatly the energy density of the present system.

Experimental

Preparation of LiCoPO4 using polyol process

$Co(COOCH_3)_2$ (Merck, 99.999%), $(NH_4)H_2PO_4$ (Sissco, 99.99%), and $LiCOOCH_3$ (Merck, 99.999%) were added to PEG (Merck, 99.999%) in a stoichiometric molar ratio of 1:1:1. The solution was heated at 250 °C for 35 h in a round bottom flask attached to a refluxing condenser. To remove PEG and partial organic compounds, the resulting solution

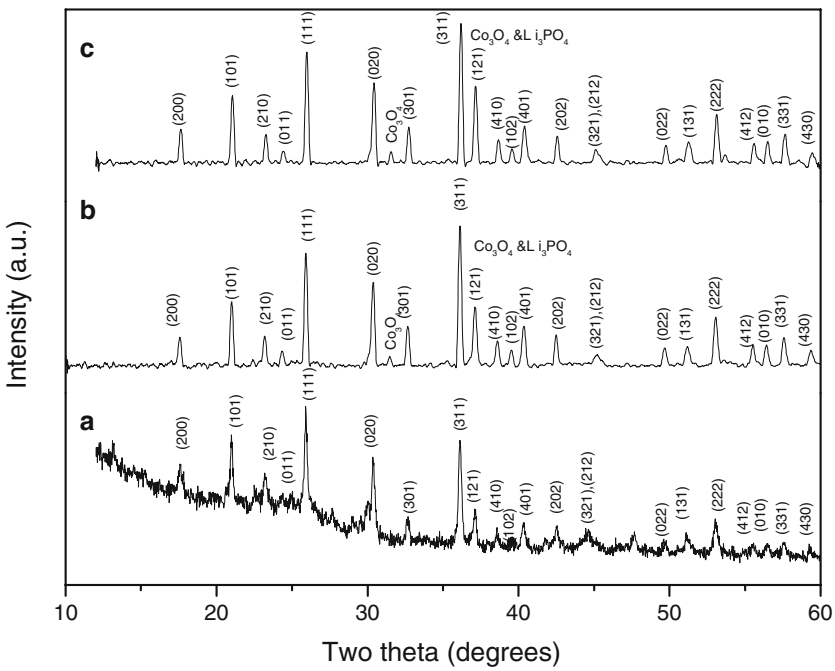

Fig. 2 X-ray diffraction patterns of $LiCoPO_4$ nanocrystalline powders: **a** sample A, **b** sample B, and **c** sample C

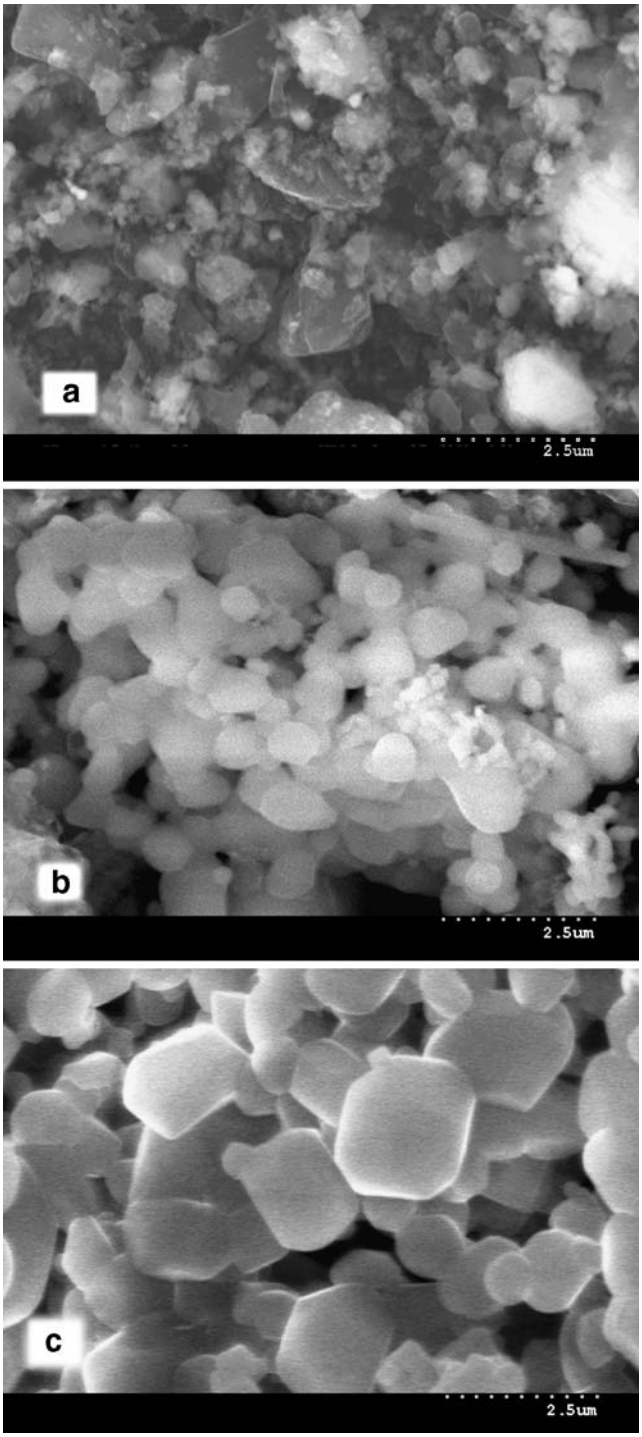

Fig. 3 SEM micrographs of $LiCoPO_4$ nanocrystalline powders: **a** sample A, **b** sample B, and **c** sample C

containing nanoparticles were washed with acetone several times. The resulting particles were separated by filtering using ceramic membrane funnels. To evaporate the water absorbed from the atmosphere, the nanoparticle powders were dried in a vacuum oven at 150 °C for 12 h. $LiCoPO_4$ nanopowders appeared black with luster. Then, the dried sample was heated to 800 °C for different time periods for 2 and 4 h, respectively. Here onwards, the dried sample,

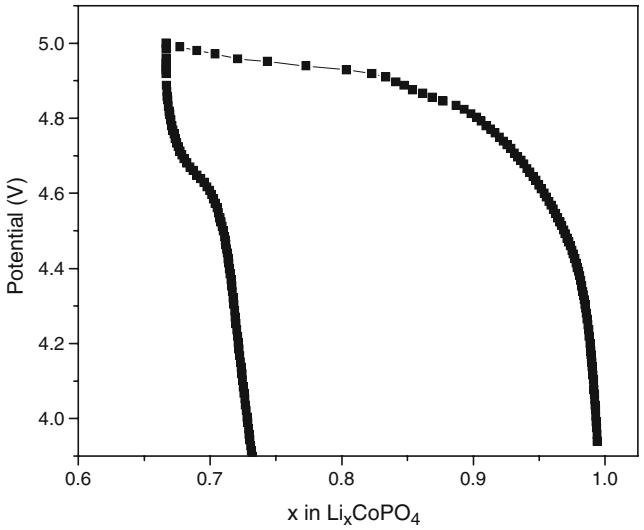

Fig. 4 Voltage–composition plot obtained from the charge–discharge of Li//$LiCoPO_4$+10 wt% carbon+10 wt% PVDF at C/10 rate

samples heated at 800 °C for 2 and 4 h will be referred as samples A, B, and C, respectively.

Characterization

Thermo gravimetry-scanning calorimetry (TG-DSC) analysis was studied using SDT-Q600 TA Instruments. The orthorhombic phase of $LiCoPO_4$ was examined by X-ray diffraction (XRD) with CuKα radiation (λ=1.54056 Å). The morphology of the samples was captured by scanning electron microscope (SEM; Hitachi, S-3000H). Electrochemical performance for the half-cell sample B is performed using swage lock cells comprising Li metal counter electrode with a 1 M solution of LiPF6 in EC/dimethyl carbonate (DMC; 1:1, *v*/*v*, Merck LP30) as the electrolyte. After assembling the cells in an argon-filled glove box, they were connected to a VPM II Biologic battery tester for either potentiostatic or galvanostatic charge/discharge tests. A capacitor test was performed using the two-electrode glass cell, consisting of a Li-ion intercalated composite as positive and CNF composite as negative electrodes. The electrode of $LiCoPO_4$ was prepared according to the following steps. The mixture containing 85 wt% $LiCoPO_4$ and 10 wt% CNF and 5 wt% *N*-methyl pyrrolidone is well mixed, and the slurry was pasted on a mild steel current collector of geometric area 1 cm^2. The negative electrode was prepared by 85% CNF with 5 wt% *N*-methyl pyrrolidone as binder. The slurry was pasted on a mild steel current collector. The electrolyte used for the test was 1 M $LiClO_4$ in EC and PC (1:1 in volume) solution. The $LiCoPO_4$ positive electrode and CNF negative electrode were dried in vacuum oven at 80°C for 12 h before assembling. The typical active material mass load ratio of $LiCoPO_4$ to CNF is 6 to 12 mg/cm^2 depended on the capacity balancing ratio of positive to negative electrodes.

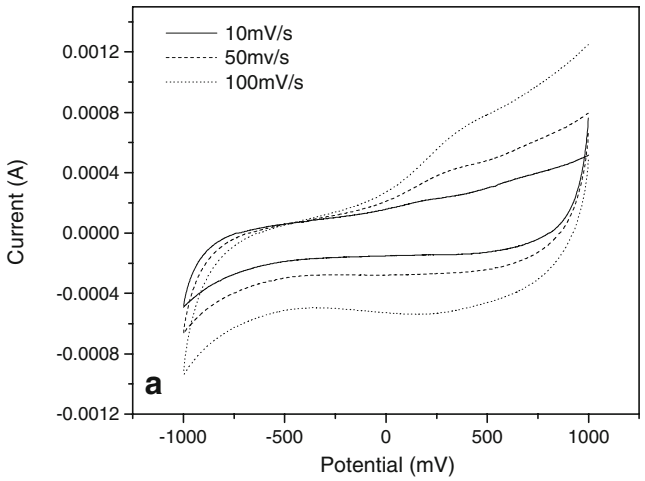

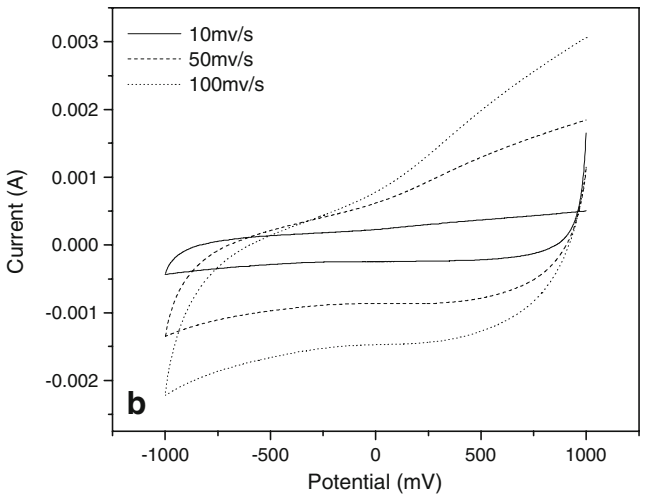

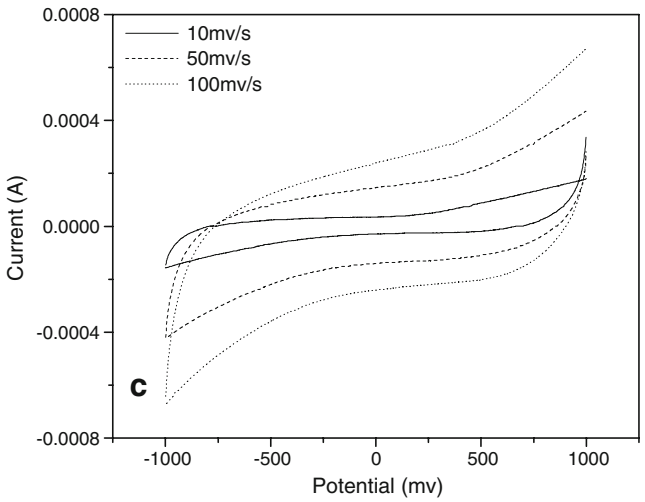

Fig. 5 Cyclic voltammetry of three hybrid cells: **a** CNF/sample A hybrid cell, **b** CNF/sample B hybrid cell, and **c** CNF/sample C hybrid cell in 1 M $LiClO_4$ EC/PC at various scan rates 10, 50, and 100 mV s^{-1}

Impedance property of the cells were characterized by EG & G Instruments (Princeton Applied Research, Model 6310). The frequency limits were typically set between 100 kHz and 0.01 Hz, and the AC oscillation was 10 mV. The cyclic voltammetry (CV) was characterized by using the electrochemical analyzer (BAS 100B). The cycle life performance of the hybrid supercapacitors were evaluated using Won-A-Tech Cycler (WBCS 3000).

Table 1 Specific capacitance of three types of hybrid cells calculated from CV curves

Sample no.	Scan rate (mV/s)	Specific capacitance (F/g)		
		CNF/Sample A hybrid cell	CNF/Sample B hybrid cell	CNF/Sample C hybrid cell
1	10	9.3	21.9	4.23
2	50	5.3	16.1	2.76
3	100	4.8	12.53	2.11

Results and discussion

Thermo gravimetry-scanning calorimetry analysis

TG-DSC analysis is studied at a ramp of 10 °C/min. Figure 1 shows the thermogram and DSC curve of $LiCoPO_4$ nanoparticles. TG shows a step-like pattern, and the sample is stable up to 420 °C proving that the sample is free from moisture and unreacted particles. A weight loss to the extent of 44 % is observed in the temperature range of 420 to 800 °C in the TG curve, and similar behavior was depicted in the DSC curve by the exothermic peak. A slight exothermic peak in DSC observed below 200 °C may be due to the decompositions of the organic products, and a large exothermic peak in DSC between 400 and 800 °C is due to the decomposition of precursor material indicating the formation of the compound.

X-ray diffraction study

Figure 2 shows the X-ray pattern of nanocrystalline $LiCoPO_4$ (a) sample A, (b) sample B, and (c) sample C. All peaks can be indexed by an olivine structure with the space group of Pnma. There was a good agreement with the $LiCoPO_4$ theoretical pattern (PDF No. 32-0552). The obtained powder was well crystalline, as the diffraction peaks were narrow and sharp. $LiCoPO_4$ contains pure olivine phase in spite of being prepared in air. With excess lithium, two additional phases Li_3PO_4 and Co_3O_4 are observed in samples B and C. This is plausible if the following reaction as reported in [13] is considered.

$$Li_{1+x}CoPO_4 + \chi/3\,O_2 \cdots \rightarrow (1-\chi/2)\,LiCoPO_4 + \chi/2\,Li_3PO_4 + \chi/6Co_3O_4$$

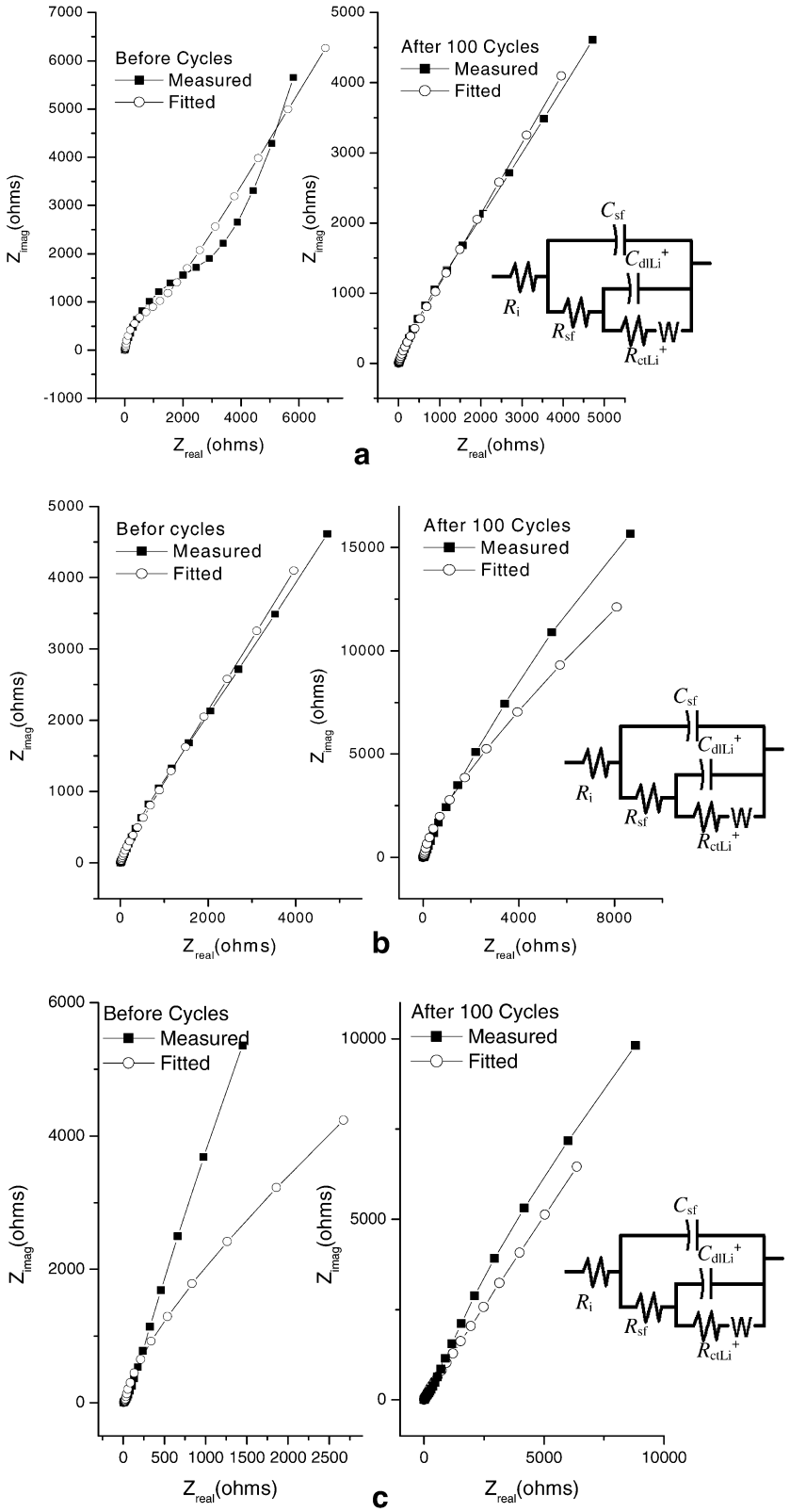

Fig. 6 AC impedance spectra of three hybrid cells: **a** CNF/sample A hybrid cell, **b** CNF/sample B hybrid cell, and **c** CNF/sample C hybrid cell before and after 100 cycles. The equivalent circuits are given in the *insert*

Sizes of $LiCoPO_4$ particles are calculated to be 55, 43, and 39 nm for samples A, B, and C, respectively from the peak at 37.2 °C by the Scherer's equation [14]. The dried powder obtained immediately after the polyol process are large in particle size when compared with the annealed samples. Furthermore, the appearance of Li_3PO_4 and Co_3O_4 phase fine particles in the annealed samples may serve as separation media that partly prevents $LiCoPO_4$ particles from direct contact with a liquid electrolyte in a cell.

Scanning electron microscopy

Figure 3 displays the SEM images of samples A, B, and C $LiCoPO_4$ nanoparticles. From the SEM micrograph of sample A, we could infer that large aggregates and irregular particle like structure are exhibited. The SEM images of samples B and C show that large aggregates are broken into small crystallites. Particles are distinct with orthorhombic and spherical shape, and the surface exhibits homogenous and smooth morphology. These particles may be several tens of nanometers to several hundreds of nanometers in size.

Electrochemical performance of the half cell

Figure 4 shows the first charge–discharge cycle of Li cell with sample A as the positive electrode. The voltage–composition curves are parallel suggesting a similar mechanism for the lithium deinsertion–insertion process. The more the excess of lithium, the better capacity retention will be obtained. The discharge capacity obtained is 40 mAh/g. Rabanal et. al.[15] had reported that at a *C*/5 rate, in the 20th cycle, the specific capacity of the carbon added material (40 Ah kg^{-1}) doubles that of the fresh material(20 Ah kg^{-1}). In view of this, the present investigation from polyol process yields double the capacity for pristine material comparable to its carbon-coated material. Therefore, $LiCoPO_4$ capacity cannot be improved without addition of carbon. However, for the first time, supercapacitors properties are explored for the $LiCoPO_4$ synthesized by polyol process without any addition of carbon.

Cyclic voltammetry

The hybrid supercapacitors are fabricated with mass-matching ratio of 2:1, CNF/$LiCoPO_4$ as mentioned in the experimental column. CV is a useful method to evaluate the intrinsic electrochemical capacitor properties of active materials. Therefore, the CV of CNF/sample A hybrid cell, CNF/sample B hybrid cell and CNF/sample C hybrid cell in the potential region between −1.0 and 1.0 V was employed to evaluate the electrochemical characteristics of the hybrid supercapacitor. Typical I–E curves at different scan rates for all the three hybrid cells are shown in Fig. 5. All the CV curves exhibit reversible, symmetric, and capacitive behavior. The CV curves of the hybrid electrodes reveal that the mechanism of electrochemical storage could be described by the electrical double-layer theory. Energy storage in these electrodes is the accumulation of ionic charge in the double-layer theory at the electrode/ electrolyte interface. This may be due to high surface area and the porosity of CNF electrode. In spite of high surface area of CNF, high capacitance could not be achieved, and this may be due to inherent capacity of the material under investigation. All the double-layer capacitance that could be obtained from the material is achieved, and this is shown below by a simple relation [16]

$$\frac{1}{C_T} = \frac{1}{C_{LiCoPO_4}} + \frac{1}{C_{CNF}} \quad (1)$$

Where C_T is total capacitance of the electrodes, $C_{LiCoPO4}$ is capacitance of $LiCoPO_4$ (55 F/g), and C_{CNF} (30 F/g) is the capacitance of CNF

$$C_T = 19.2\,F$$

Theoretical capacitance value calculated using the above-mentioned relationship matches quite well with the capacitance calculated from CV curve of CNF/sample B

Table 2 Summaries of the fitting results of internal resistances (R_i), surface capacitances (C_{sf}), surface film resistances (R_{sf}), charge-transfer resistances for Li^+ intercalation $R_{ct}Li^+$, and double layer capacitances for Li^+ intercalation $C_{dl}Li^+$ for (1) CNF/sample A hybrid cell (2) CNF/sample B hybrid cell, and (3) CNF/sample C hybrid cell before and after 100 cycles based on a series of experimental results

Types of hybrid cells	R_i (Ω)		C_{sf} (F)		R_{sf} (Ω)		$C_{dl\ Li+}$ (F)		R_{ctLi+} (Ω)	
	Before cycle	After 100 cycles	Before cycle	After 100 cycles	Before cycle	After 100 cycles	Before cycle	After 100 cycles	Before cycle	After 100 cycles
1	7.96	6.52	1.41×10^{-5}	1.07×10^{-5}	5.34×10^{-4}	18.46	3.5×10^{-5}	6.89×10^{-7}	892.4	0.01
2	8.62	11.17	1.48×10^{-5}	4.53×10^{-5}	22.67	44.98	0.7078	2.6×10^{-4}	0.03	1.03×10^{-7}
3	6.45	7.34	1.12×10^{-4}	6.38×10^{-6}	21.41	2.58×10^{-4}	9.01×10^{-3}	1.62×10^{-5}	0.051	0.01

hybrid cell, which is mentioned later. From the CV curves, specific capacitance parameter could be obtained using

$$C_m = I/\text{Scan rate}\, m \quad (2)$$

where I is the current and m is the mass of active material. Table 1 shows specific capacitance value obtained for three hybrid cells at various scan rates. As scan rate increases C_m decreases for all the three hybrid cells.

The CV curves reveal that the capacitance characteristic is distinguished from that of the electric double-layer capacitance in which case it is normally close to an ideal rectangular shape, indicating that the measured capacitance is mainly a pseudocapacitance. This is low enough to be a good supercapacitor electrode material. However, redox peak behavior is not observed obviously. Redox behavior may be due to Co^{3+}/Co^{4+} from smaller amount of Co_3O_4 phase formed along with $LiCoPO_4$. The capacitance observed with samples A and C is low, and this may be due to the pure double-layer capacitance of the synthesized material $LiCoPO_4$. However, in sample B, the total capacitance is due to the combined capacitance of double layer and redox capacitance. Redox capacitance is obtained from the phase Co_3O_4 in addition to small redox capacitance due to insertion/extraction of Li ions in $LiCoPO_4$. Co^{3+}/Co^{4+} redox capacitance in sample B is substantial, and this is to be tapped and further scope of work is toward the increasing Co_3O_4 phase along with $LiCoPO_4$ phase wherein Li_3PO_4 phase protects Co_3O_4 and acts as a separation media that partly prevents $LiCoPO_4$ particles from degradation from the electrolyte. Although sample C has both Li_3PO_4 and Co_3O_4 phase, yet, surface resistance, R_{sf}, increases after few cycles as reported in electro chemical impedance spectroscopy analysis.

Electrochemical impedance spectroscopy analysis

The spectra in the typical form of Nyquist plots (Z' vs Z'') of hybrid supercapacitor cells are shown in Fig. 6. The electrochemical impedance measurement was carried out at different potential conditions in the frequency range of 10^5 to 10^{-2} Hz. Impedance spectra of the three types of hybrid cells before and after 100 cycling is recorded. A semicircle with a Warburg behavior for sample A and a depressed semicircle for sample B and the Warburg alone is observed for sample C. A good fit is obtained using the equivalent circuit of $R(C(R(C\,(RW))))$ for all the three hybrid cells. The fitting results of internal resistances (R_i), surface film resistances (R_{sf}), charge-transfer resistances for Li^+ intercalation R^+_{ctLi}, surface film capacitances (C_{sf}), and double-layer capacitances for Li^+ intercalation C^+_{dlLi} for (1) CNF/sample A hybrid cell, (2) CNF/sample B hybrid cell, and (3) CNF/sample C hybrid cell before and after 100 cycles based on a series of experimental results are tabulated in Table 2.

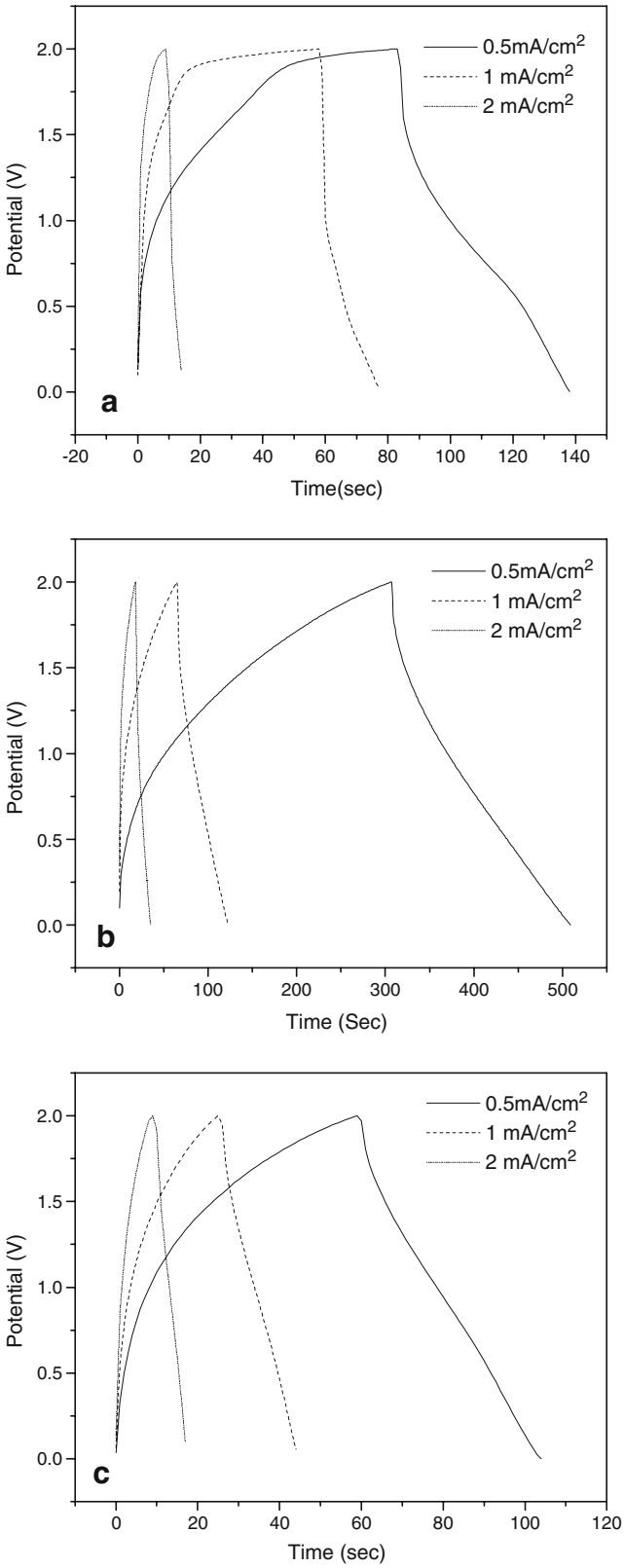

Fig. 7 Charge–discharge curves of the three hybrid supercapacitors at different current rates 0.5, 1, and 2 mAcm^2 for: **a** CNF/sample A hybrid cell, **b** CNF/sample B hybrid cell, and **c** CNF/sample C hybrid cell

R_i values for all the three hybrid cells ranging from 6 to 11 Ω is a positive factor for an ultracapacitor to yield higher capacitance. On comparing the R_{sf} of all the three cells, CNF/sample B hybrid cell and CNF/sample C hybrid cell are low in the range 20 Ω approximately. Absence of Li_3PO_4 and Co_3O_4 phase in sample A produces a high surface resistance of 50 kΩ before cycling, and surface resistance is reduced considerable to 18 Ω after 100 cycles. Whereas, the R_{sf} value for CNF/sample C hybrid cell had increased considerably to 20 kΩ after 100 cycles can be attributed to poor diffusion of Li ions. Therefore, capacity retention of CNF/sample C hybrid cell should be poor. However, $R^{+}_{ctLi}$for CNF/sample A hybrid cell and CNF/sample C hybrid cell after 100 cycles were 10^{-2} Ω, respectively. $R^{+}_{ctLi}$for CNF/sample B hybrid cell is 10 μΩ.

The surface film capacitance and double-layer capacitance for all the three type of hybrid cells are in microfarads. Cheng et al. had reported that the R_i, R_{sf}, and R_{ct} values for pure LTO [17] were 55.4, 133.5, and 993.9 Ω, respectively. Best performing CNF/sample B hybrid cell having R_i, R_{sf}, and R_{ct} values as 8.62, 22.67, and 1.03×10^{-7} Ω, respectively. $LiCoPO_4$ nanoparticles synthesized by polyol process offers less resistance than LTO.

Rate capability

Figure 7a–c shows the charge/discharge curves of CNF/sample A, CNF/sample B, and CNF/sample C hybrid cells with a mass ratio of 2:1 between 2 and 0 V at various current density from 0.5 to 2 mA/cm^2. The curves are almost linear, and the sudden drop of potential at the beginning of charge and discharge is associated with the ohmic resistance of the cell. The average internal resistance of the capacitor can be evaluated by the equation as follows

$$R = V_{\text{charge}} - V_{\text{discharge}}/2I \tag{3}$$

where V_{charge} is the cell voltage at the end of charge, $V_{\text{discharge}}$ is the cell voltage at the beginning of the discharge, and I is the applied current. This gives an average value of 270, 191, and 85 Ω for CNF/sample A, CNF/sample B, and CNF/sample C hybrid cells, which includes the electrode resistance and the electrolyte solution resistance.

Capacitance of the hybrid is calculated as follows

$$C_m = I\,t/\Delta V\,m \tag{4}$$

where I is the current of charge–discharge and t is the time of discharge, ΔV is the discharge voltage difference between the t period, and m is the mass of active materials within the hybrid, which includes both positive electrode and negative electrode. Table 3 shows the specific capacitance and the internal resistance, R, calculated from discharge curves of the three types of hybrid cells. Specific

Table 3 Specific capacitance and internal resistance of (1) CNF/sample A hybrid cell, (2) CNF/sample B hybrid cell, and (3) CNF/sample C hybrid cell calculated from discharge curves

Type of hybrid cell	I (mA)	Specific capacitance (F/g)	$R=V_{\text{charge}}-V_{\text{discharge}}/2I$ (Ω)
1	0.5	5.19	360
	1.0	3.46	250
	2	2.30	200
2	0.5	19.03	200
	1	10.96	200
	2	7.69	173
3	0.5	4.23	40
	1	3.65	25
	2	3.07	20

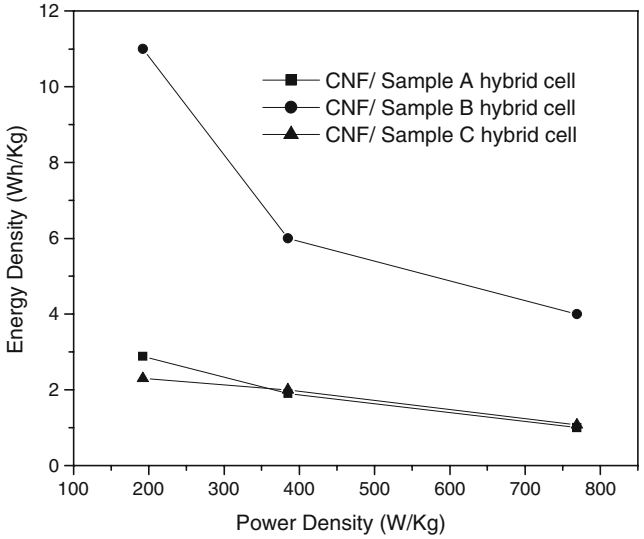

Fig. 8 Ragone plots of the three types of hybrid cells

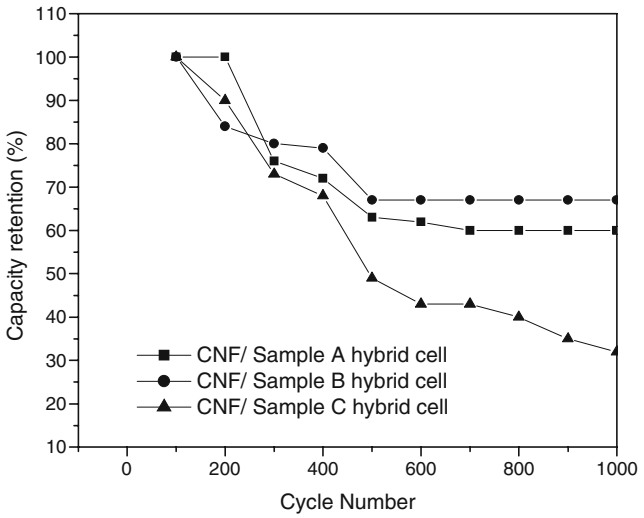

Fig. 9 Cycling profile of the three types of hybrid cells at a current density of 0.5 mA/cm^2

capacitance value calculated theoretically, from CV curves and from discharge curves for CNF/sample B hybrid cell, were approximately equivalent to 19 F/g.

From E–I curves, it is observed that these hybrid electrodes behave as good capacitor electrode, and hence, this material ($LiCoPO_4$) is a suitable supercapacitive active electrode material. Increased capacitance in the sample B may be due to Co_3O_4 phase in addition to Li intercalation, as discussed earlier and may also be due to defect rich Co_3O_4, which may help in movement of ions. In the case of Co_3O_4, the deviations in cobalt to oxygen ratio lead to empty oxygen sites. These sites are potential wells that can trap either one or two electrons. In addition to this interstitial occurrence of cobalt ions, which are shallow donors, promotes the ionic conductivity. Oxygen vacancies create deep level of donors. These create much extrinsic defects. In the present investigation, the preparation conditions of the hybrid electrode helps in getting high defect content of Co_3O_4 with CNF in increasing charge carriers and enhancing double-layer capacitances. Although in sample C, Co_3O_4 and Li_3PO_4 phase are found, yet, specific capacitance realized was 4.23 F/g, and this is due to high surface film resistance, R_{sf}, 20 kΩ after 100 cycles as mentioned before.

Figure 8 gives Ragone plots of the three types of hybrid cells with a mass ratio of 2:1 between 2 and 0 V. The specific power density P and energy density E of the hybrid supercapacitor are calculated as mentioned below

$$P = \Delta \mathrm{E}\, I/m \tag{5}$$

$$E = P\, t \tag{6}$$

$$\Delta \mathrm{E} = \mathrm{E}_{\max} + \mathrm{E}_{\min}/2 \tag{7}$$

where E_{max} is the potential at the beginning of discharge and E_{min} is the potential at the end of the discharge.

Figure 8 shows that CNF/sample A hybrid and CNF/sample C hybrid have maximum energy density of 2.5 and 2.9 Wh/kg at power density of 192 W/kg, respectively. The energy density increases from 5 to 11 Wh/kg when the power density decreases from 770 to 192 W/kg for CNF/sample B hybrid cell.

Thierry et al. [18] had reported that Fe_3O_4/MnO_2 capacitor cycled between 0 and 1.8 V had real energy density of 7 Wh/kg at power density of 820 W/kg. In our work, CNF/sample B hybrid cell had delivered a maximum energy density of 11 Wh/kg at power density of 192 W/kg in the potential window of 0 to 2 V.

Figure 9 compares the cycling profile of the hybrid cells at a current of 0.5 mA/cm^2. Both CNF/sample A and CNF/sample B hybrid cells exhibit good cycling life with a capacity retention of 67 % over 1,000 cycles.

Conclusion

In this investigation, we have presented a non-aqueous electrochemical supercapacitor technology using $LiCoPO_4$ as positive electrode and CNF as negative electrode in 1 M $LiClO_4$ in EC/PC non-aqueous electrolyte. Nanocrystalline powders of $LiCoPO_4$ were synthesized by polyol process, and resultant powders were heat-treated at 800 °C for different time periods of 2 and 4 h. All the three samples were characterized by physical and electrochemical technique. The sample heated for 2 h at 800 °C had delivered the maximum specific capacity of 19 F/g than other two samples. Maximum energy density of 11 Wh/kg at 192 W/kg was obtained. The growth of Co_3O_4 and Li_3PO_4 defect in sample B has played great role for the depletion of electrode from electrolyte. Despite the limited energy density and power density obtained, we have made the feasibility of hybrid device using pristine olivine, $LiCoPO_4$.

Acknowledgement The first author highly acknowledges Council for Scientific and Industrial Research, CSIR, New Delhi, for the grant of Research Associate Fellowship and Department of Science and Technology, DST, New Delhi, for meeting the Travel grant to present the work in international Conference, ICMAT 2007, Singapore.

Reference

1. Lackner AM, Sherman E, Braatz PO, Margenum JD (2002) J Power Sources 104:1
2. Faggioli E, Rena P, Danel V, Andrieu X, Mallant R, Kahlen H (1999) J Power Sources 84:261
3. Lipka SM, Reisner DE, Dai J, Cepulis R (2001) In: Proceedings of the 11th International Seminar on Double Layer Capacitors, Florida Educational Seminars
4. Amatucci GG, Badway F, Pasquier AD, Zheng T (2001) J Electrochem Soc 148:A930
5. Amatucci GG, Tarascon JM, Klein LC (1996) J Electrochem Soc 143:1114
6. Pasquier AD, Plitz I, Gural J, Badway F, Amatucci GG (2004) J Power Sources 136:160
7. Wang YG, Xia YY (2006) J Electrochem Soc 153(2):A450
8. Wang YG, Luo JY, Wang CX, Xia YY (2006) J Electrochem Soc 153(8):A1425
9. Bramnik NN, Bramnik KG, Baehtz C, Ehrenberg H (2005) J Power Sources 145:74
10. Wolfenstine J, Allen J (2004) J Power Sources 136:150
11. Huang X, Ma J, Wu P, Hu Y, Dai J, Zhu Z, Chen H, Wang H (2005) Mater Lett 59:578
12. Poul L, Ammar S, Jouini N, Fievet F, Villain F (2001) Solid State Sciences 3:31
13. Shui JL, Yu Y, Yang XF, Chen CH (2006) Electrochem Commun 8:1087
14. Zheng K, Alexandrov IV, Kilmametov AR, Valiev RZ, Lu K (1997) J Phys D Appl Phys 30:3008
15. Rabanal ME, Gutierrez MC, Garcia-Alvarad F, Gonzalo EC, Arroyo-de Dompablo ME (2006) J Power Sources 160:523
16. Pell WG, Conway BE (2004) J Power Sources 136:334
17. Cheng L, Li XL, Liu HJ, Xiong HM, Zhang PW, Xia YY (2007) J Electrochem Soc 154(7):A692
18. Brousse T, Belanger D (2003) Electrochem Solid State Lett 6(11): A244